A Study of Slip Ratios for the Flow of Steam-Water Mixtures at High Void Fractions

WILLIAM H. VANCE and R. W. MOULTON

University of Washington, Seattle, Washington

A technique employing the impulse plate principle was developed whereby the ratio of the average vapor-to-liquid velocities (slip ratio) for flowing two-phase mixtures could be measured accurately at high vapor volume fractions. Data were collected for steam-water mixtures flowing adiabatically in a horizontal ½-in. tube. Flow conditions were in the spray annular and dispersed flow regimes and covered a pressure range of 30 to 80 lb.$_f$/sq.in.abs., flow rates of 200 to 800 lb.$_m$/(sec.)(sq.ft.), and steam qualities of 0.02 to 0.8. The experimental slip ratios, ranging between 1 and 3.5, decreased with increasing quality and pressure and increased with increasing mass velocity and pressure gradient.

A theoretical analysis in which an idealized dispersed flow model was used indicated that the observed average slip ratios were caused largely by local slip between vapor and entrained droplets and that high local slip ratios may be attained near critical flow rates due to the simultaneously occurring steep pressure gradients.

The total pressure gradients, computed by adding the Martinelli-Nelson frictional pressure drop prediction to the acceleration pressure gradients calculated by the use of an empirical correlation of the slip ratio data, deviated from the experimental values by an average of only 14%.

The flow of vapor-liquid mixtures in conduits has found more and more frequent application in recent years, particularly in the fields of cryogenics, nuclear energy, and space technology. Due to the immediate need for design procedures, many of the data and correlations have been of a grossly empirical nature and have contributed little to a better understanding of the basic mechanisms governing two-phase flow.

Within the last several years, therefore, the emphasis has been on putting the study of two-phase flow on a firmer theoretical foundation, and much effort has been directed toward the investigation of such fundamental aspects as the nature of bubble formation and growth in boiling liquids (*1, 2*), the relative distribution of liquid and vapor over the flow cross section (flow pattern) (*3* to *5*), the proportion of the conduit cross section occupied by the vapor phase (void fraction) (*6, 7*), and the critical or maximum flow of two-phase, single-component systems (*8* to *10*), similar to the sonic flow phenomenon observed in gases.

Bubble and droplet dynamics have been the objects of some analytical studies (*11* to *13*), but there have been very few direct investigations of the relative motion between the two phases. Similarly, the possibly important role of metastable or nonequilibrium conditions in rapidly accelerating two-phase flow has received attention from very few recent investigators (*14*).

Relative motion between two phases usually is studied in terms of the slip ratio, which in this case is the ratio of the average vapor velocity to the average liquid velocity at a particular cross section of the flow. This term has the advantage of being dimensionless as compared to the difference in the average phase velocities, termed the slip velocity, which is sometimes used.

William H. Vance is with Bettis Atomic Power Laboratory, Pittsburgh, Pennsylvania.

Many studies have been made of the void fraction, from which the slip ratio is readily computed, in both one- and two-component vapor-liquid flow (*15*). However the radiation attenuation technique usually employed in these investigations is reasonably accurate only in the range of low to medium values of the void fraction. Only two previous investigations (*16, 17*), using other methods, produced suitable data at high void fractions, and the range of their experiments was limited.

Most of the data analyses have dealt directly with the void fraction rather than the corresponding slip ratio, primarily because of the immediate relationship of the void fraction to the nuclear properties of the coolant in boiling water nuclear reactors. However the slip ratio is a much more sensitive measure of the departure from the idealized homogeneously mixed flow and is therefore a more revealing as well as convenient parameter for analysis.

Almost no data exist then on slip ratios at void fractions greater than 0.8. At pressures less than 100 lb./sq. in. abs., this corresponds to practically the entire range of vapor quality (from 0.02 to 1.0). This region, usually referred to as wet steam, has recently become important in the design of advanced nuclear reactors which use this medium as the coolant (*18*).

The present research was undertaken in a effort to fill this gap in our knowledge and to gain an insight into the mechanism of vapor-liquid slip and its role in two-phase flow systems.

BASIC CONSIDERATIONS

Turbulent vapor-liquid flow in conduits is an extremely complex process, and any attempt to develop a generalized theory, including all of the many intricate combinations of conditions, would meet with prohibitive difficulties. Therefore, to explain and correlate the important design parameters, such as pressure gradient, void fraction, and critical

flow rate, certain simplifying assumptions are necessary which usually restrict the range of application of the final results. In this work the following assumptions were made.

1. The mass, energy, and momentum equation can be written separately for each phase in terms of the area weighted average phase velocities. Thus the final results will express only the average slip and will not distinguish between local slip (actual slip between entrained droplets and surrounding vapor) and apparent slip due to a greater concentration of liquid in the lower velocity region near the conduit wall (annular or spray annular flow pattern).
2. Thermodynamic equilibrium is maintained, and the thermodynamic properties of the saturated liquid and vapor are given by Keenan and Keyes' steam tables (*19*).
3. Temperature and pressure are constant over any cross section of the flow.

The separate phase mass balance equations and the total energy balance equation for horizontal, adiabatic, two-phase flow based on these assumptions are derived in the Appendix.

Impulse Plate Principle

The impulse plate principle, illustrated in Figure 1, formed the basis of the experimental slip ratio determinations (see references *16, 23, 24,* and 33 for previous applications of this principle). The fluid mixture emerging from the tubular test section and impinging on the vertically suspended impulse plate is forced by structural elements of the apparatus (not shown) to leave the region of the plate only in directions perpendicular to the original flow axis. The momentum force of the flowing fluid at the exit of the tube is given by

$$F_1 = \frac{1}{g_c}(w_g u_g + w_l u_l)_1 \tag{1}$$

If a compressible single-phase fluid were flowing in the same situation with sonic flow conditions existing at the exit, the static pressure at the throat P_1 could be greater than the back pressure in the immediate vicinity of the impulse assembly P_2 (a pressure discontinuity would occur in the free jet downstream of the throat). It is not certain that a sonic two-phase flow exactly analogous to the single-phase case actually exists, but assuming that it does, a force balance over the control volume indicated by the dashed lines in Figure 1 gives

$$F_1 = F_2 - A(P_1 - P_2) \tag{2}$$

where F_2 is the force required to hold the impulse plate stationary.

However all the experimental data analyzed in this paper were at subcritical flow rates (several critical flow runs were made for comparison). Therefore, when we assume that an analogy with the case of single-phase jets can be drawn, P_1 should equal P_2 (see reference *48* for a detailed analysis of such a situation in single-phase flow). Following Equation (2) then, all calculations were made on the assumption that F_1 equals F_2.

Experimental support for this assumption was also obtained. A pressure gauge located at the rear of the expansion chamber provided an estimate of P_2 for comparison with P_1. Run No. 25, the pressure profile for which is included in Figure 10, was one of only six runs where P_2 was measurably less than P_1. In this case the difference was 0.3 lb./sq. in., which if accounted for in Equation (2) would have increased the slip ratio for this run by 9%. Only two other runs (13 and 29) produced P_2 values resulting in larger apparent errors in the experimental slip ratio. Since the estimate of P_2 provided by the pressure gauge was of questionable accuracy, and since in over 80% of the runs there was no detectable difference, the assumption that P_2 equals P_1 was felt to be justified.

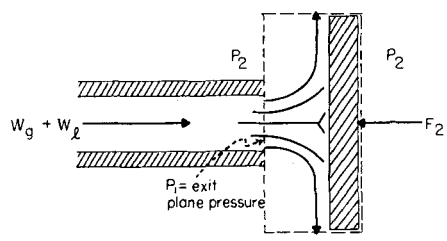

Fig. 1. Impulse plate principle.

Calculation of the Slip Ratio

Substitution of the mass balance expressions for the average phase velocities [Equation (A-6) and (A-7) of the Appendix] into Equation (1) yields a quadratic equation for the slip ratio, from which the quadratic formula gives

$$k = \frac{B - \sqrt{B^2 - 4v_g/v_l}}{2} \tag{3}$$

where

$$B = \frac{\frac{g_c F}{AG^2} - x^2 v_g - (1-x)^2 v_l}{x(1-x)v_l} \tag{4}$$

It can be readily shown by calculations at $k = 1$ that the negative sign is the correct one to use in the quadratic formula.

Equation (3) and the total energy balance, Equation (A-12), may be solved simultaneously for the quality and slip ratio at the exit plane of the test section, if the other terms are known at the same point. The stagnation enthalpy was determined from upstream measurements of the enthalpy and flow rate of the liquid and vapor streams before they were mixed. The data also included values for the quantities A, G, and F as well as the pressure at the exit plane, from which the thermodynamic properties were obtained in conjunction with assumption 2 above.

Two-Phase Pressure Drop

Isbin, Moen, and Mosher (*20*) presented the total momentum balance for two-phase flow in a constant area, horizontal tube:

$$A\,dP + (dF_l + dF_g) + \frac{1}{g_c} d(w_g u_g + w_l u_l) = 0 \tag{5}$$

where the second term represents the net force expended by the liquid and vapor phases in overcoming frictional resistance. After substituting for w and u from the mass balance equations in the Appendix and integrating, one can transform Equation (5) to

$$\Delta P_{TP} - \Delta P_{TPF} - \Delta P_a = 0 \tag{6}$$

where

$$\Delta P_a = \frac{G^2}{g_c} \Delta \left\{ \left[\frac{x v_g}{k} + (1-x)v_l \right] \left[1 + x(k-1) \right] \right\} \tag{7}$$

Once the slip ratio is known, Equation (7) gives the acceleration pressure drop, and subtraction from the total measured pressure drop yields the pressure loss due to friction.

DESCRIPTION OF APPARATUS

A schematic diagram of the flow system is given in Figure 2. Steam and water supplied by the main university lines were brought together in the mixing section to produce a two-phase mixture of the desired quality. This was flashed through the horizontal test section into the expansion chamber,

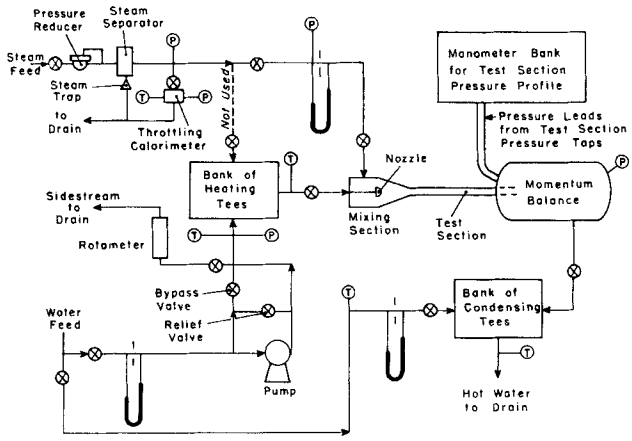

Fig. 2. Schematic diagram of apparatus.

where the forward momentum of the stream was measured. The mixture leaving the expansion chamber was condensed with cold water in the condensing tees, and the effluent was flushed down the drain. The entire apparatus was heavily insulated to insure adiabatic flow conditions.

In the mixing section a nozzle sprayed the cold water at high speed in a 45 deg. hollow cone pattern into the steam which flowed around and from behind the nozzle. The thin jets of water were broken up and intimately mixed with the steam, and the mixture flowed through a conical section which smoothly reduced the flow area down to that of the test section. Based on Mosher's experience (*21*), a 1½ in. thick section of aluminum honeycomb material was fitted into the mixing cone to promote mixing and to assure the attainment of thermodynamic equilibrium.

Test Section

By use of a deep-hole drilling rig and special machining techniques, a perfectly straight, smooth walled test section of constant cross-sectional area was produced from a 1-in. diameter 303 stainless steel rod.

Eleven pressure taps were drilled with a No. 80 wire twist drill (0.0125 in. in diameter) with a steel insert in the tube bore to inhibit burr formation. Alternate polishing of the tube bore and redrilling of the pressure taps assured the absence of burrs in the final test section. The great care exercised to avoid burrs was based on experiments by Rayle (*22*) who demonstrated the necessity of such precautions to achieve precision pressure measurements in high-speed flow systems.

The end of the test section was turned off on a lathe to bring the last tap as close as possible to the exit, thus facilitating the accurate extrapolation of the pressure profile to obtain the exit plane pressure necessary for the slip ratio calculations. The final distances of the pressure taps from the tube exit plane, accurate to ± 0.001, were 0.031, 0.064, 0.099, 0.148, 0.244, 0.440, 0.921, 1.927, 3.917, 7.926, and 15.934 in., the location of each successive tap being rotated 45 deg. around the circumference of the tube. The final test section had an overall length of 22 in. and an inside diameter of 0.5045 in.

Impulse Measuring System

The design of the momentum balance, shown in detail in Figure 3, was based principally on similar apparatus constructed by Giffen and Crang (*23*) and by Linning (*16*). The forward motion of the fluid leaving the test section was arrested in the momentum cage where stainless steel wire screens dispersed the jet and prevented splashback. The surrounding cage of annular rings and spacers forced the fluid to leave in a direction perpendicular to the original flow axis, after which it flowed out the bottom of the expansion chamber to the condensing section. The expansion chamber was large so that frictional and induction effects on the jet were negligible.

The impulse rod and momentum cage unit (impulse assembly) was suspended by two nichrome wires from the top of the expansion chamber (Figure 3), allowing the assembly to swing freely in the perpendicular plane intersecting the test section axis. The force of the fluid jet on the impulse

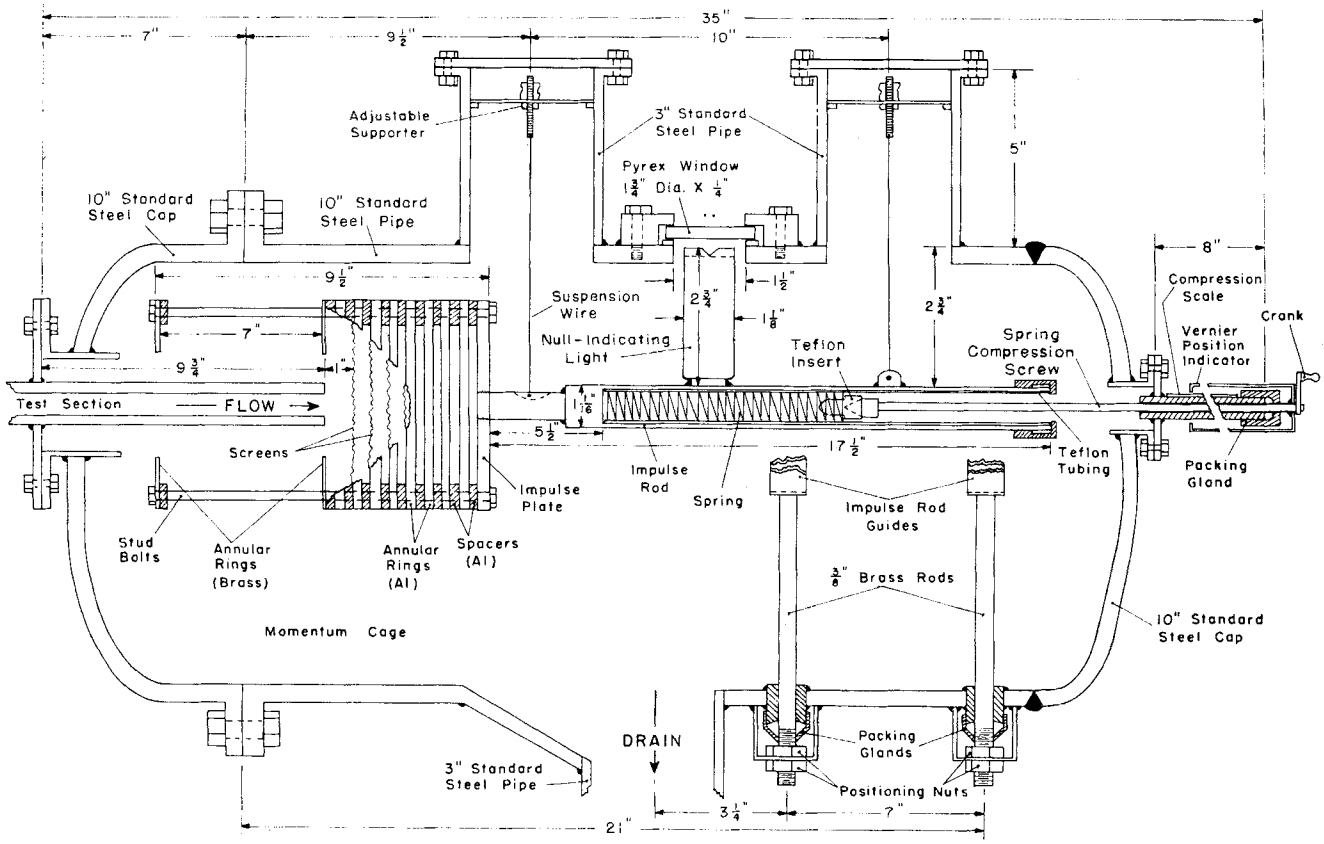

Fig. 3. Details of momentum balance.

assembly was counteracted by turning the spring compression screw at the rear of the expansion chamber, thereby compressing the impulse spring and maintaining the impulse assembly at the null (no load) position.

The position of the impulse assembly was determined by means of a null indicating system which greatly magnified any displacement from the null point so that a movement of a few thousandths of an inch was easily discernible. The compression of the spring was read directly from a vernier scale constructed as a part of the spring compression screw at the rear of the expansion chamber.

Instrumentation and Calibration

The water and steam flow rates were measured by orifice meters which were calibrated by direct time-weight measurement techniques. The feed steam enthalpy was determined by means of a throttling calorimeter. Thermometers and calibrated copper-constantan thermocouples located in deep copper tubing wells were employed to measure temperatures in the apparatus.

Pressure measurements were obtained with high accuracy Bourdon tube gauges which were periodically calibrated on a dead-weight tester. The locations of the temperature and pressure measurement points in the apparatus are indicated in Figure 2. The pressure profile over the last 2 in. of the test section was accurately determined by a bank of seven mercury manometers connected in series to the last eight pressure taps to give the pressure differences between adjacent taps. A Helicoid gauge ($\pm$ 0.25% accuracy) on the last tap before the test section exit provided the absolute pressure level for the profile. The pressure profile was extrapolated graphically to obtain the exit plane pressure.

The equipment was successfully operated using single-phase flow in the system, and the theoretical impulse force varied linearly with the measured spring compression as expected. However, frictional and mechanical effects in the momentum balance, although reduced to a minimum by the use of Teflon parts, gave rise to a significant "pseudo hysteresis" effect which prevented the use of a single spring calibration for the two-phase experiments.

A special technique consequently was developed wherein the momentum apparatus was rebalanced with cold water flow immediately after each two-phase run, maintaining the spring under approximately the same compression force at all times. Calibration runs with cold and hot water demonstrated that thermal effects due to the large temperature difference between the two-phase runs and the water rebalance could be neglected.

EXPERIMENTAL RESULTS

The experimental slip-ratio data are shown in Figure 4 plotted against the homogeneous quality x^o. Also shown in Figure 4 are Linning's results (*24*), the only data reported in the literature at conditions close to those of the present work.

The experimental mass velocities ranged from 200 to 800 lb./(sec.) (sq. ft.), the exit pressures from 25 to 80 lb./sq. in. abs., and the exit liquid volume fractions from 0.0004 to

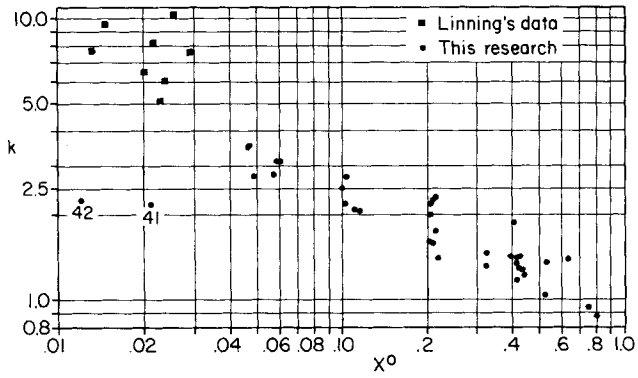

Fig. 4. Experimental slip ratios vs. homogeneous quality.

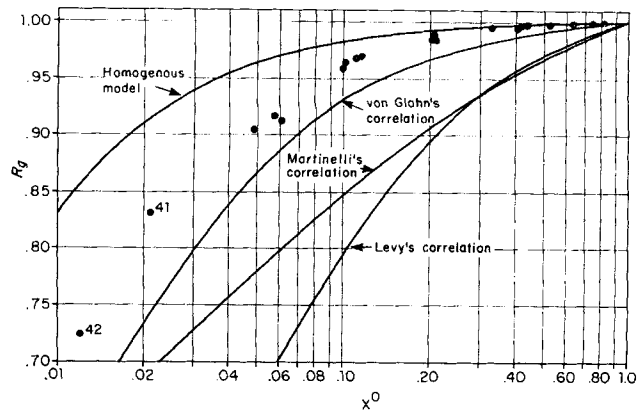

Fig. 5. Comparison of experimental void fraction data with Martinelli, Levy, and von Glahn correlations and homogeneous model at P = 50 lb.$_f$/sq.in.abs.

0.28. The original data and the computer calculation techniques are available (*25*).

The results may also be presented in the form of void fraction rather than slip ratio, using Equation (A-8) to make the conversion. Twenty-three of the experimental runs were at an exit pressure of around 50 lb./sq. in. abs. The measured void fractions for these runs are compared with those predicted by the homogeneous model (k = 1) and the correlations of Martinelli (*26*), Levy (*27*), and von Glahn (*28*) in Figure 5.

It is seen that even the much abused homogeneous model comes closer to the observed void fractions than either Martinelli's or Levy's correlations. Von Glahn's purely empirical correlation does about as well as the homogeneous model, except at void fractions above 0.99 (corresponding to qualities greater than 0.2 at 50 lb./sq. in. abs.), where the observed slip ratios do not significantly change the void fractions from those predicted by the homogeneous model.

The inability of these three correlations to predict the present results is not too surprising, since they were based almost exclusively on data at void fractions less than 0.8. It should be pointed out that, in direct conflict with the experimental results of this research, all three correlations predict ever increasing slip ratios greater than unity as the steam quality approaches one. Several other promising void fraction correlations have appeared recently (*42, 43*); however most of the present data lie outside their range of variables and a meaningful comparison was not possible.

Experimental Errors

The greatest sources of error in the final slip-ratio results were inaccuracies in the impulse force, exit pressure, and steam flow rate measurements, the relative influence of each being dependent on the total mass flow rate and the quality.

At high qualities (above 50%) the calculated slip ratio was quite sensitive to variations in the steam flow rate. It was estimated that the slip-ratio error due to uncertainty in the steam flow rate ranged from 5% at the low qualities to 12% at the high qualities, with an average error of about 7%.

The largest source of error for the runs at high flow rates was the exit pressure determination. This was due to the large, rapidly changing pressure gradients which occurred near the end of the test section at high rates of flow, preventing an accurate extrapolation of the pressure profile to the exit plane. For this reason no experiments could be successfully carried out at critical flow conditions where the pressure gradients were the greatest. At the highest flow rates used the maximum error in the exit plant pressure could have been as high as 2 or 3 lb./sq. in. with a corresponding slip-ratio error of 15 to 20%. For over three quarters of the runs, however, the error in the exit pressure determination was less than 1 lb./sq. in. corresponding to a slip-ratio error of 5% or less.

The variation in the calculated slip ratio due to inaccuracy in the impulse force measurement could be analyzed directly by using the basic equations to compute the function dk/dF

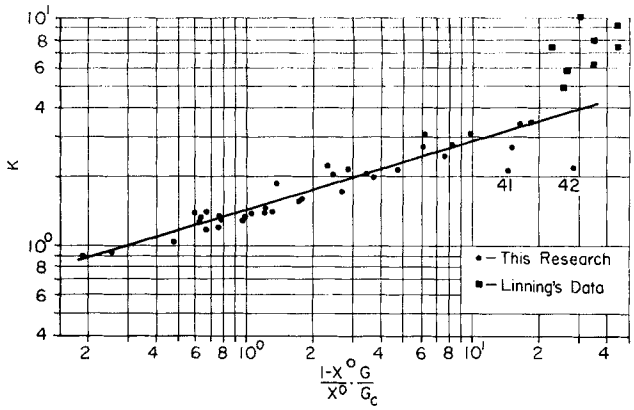

Fig. 6. Empirical slip-ratio correlation.

for each run. The impulse force measurement was estimated to be accurate to better than ± 0.1 lb., and the corresponding maxmum possible error in the slip ratio averaged 3.1% for all runs with a maximum of 9.7%.

Analysis of Slip-Ratio Results

The mixture quality was found to be the most important parameter affecting the experimental slip ratios (Figure 4). Cross plotting showed that the slip ratio generally increased with increasing mass velocity and decreased with increasing pressure. These effects were surprisingly small, however, and the scatter in the data resulted in many inconsistencies.

In searching for a suitable empirical correlation of the data reflecting the observed pressure and mass velocity effects, we investigated several of the approaches and parameters used by previous workers to correlate void fractions or slip ratios, including the use of the Martinelli parameter χ_{tt} (*26*). All methods produced more scatter than the simple quality plot of Figure 4.

It was noted that at constant quality, the slip ratio generally increased as the pressure gradient at the test section exit increased. Steep exit pressure gradients are associated with flow rates approaching critical flow, and a logical quantity descriptive of this condition is the ratio of the actual mass velocity to the critical mass velocity at the same pressure and quality.

To evaluate this ratio the critical flow rate correlation of Faletti and Moulton (*8*) was used, wherein the ratio G_c/G_{TH} is presented as an empirical function of the homogeneous quality. Faletti employed horizontal adiabatic test sections under operating conditions quite similar to those used in this work, and his correlation has been verified closely by Zaloudek (*10*).

The theoretical critical flow rate from the homogeneous model was calculated from the following empirical equation developed by Faletti from steam table data:

$$G_{TH} = 96.2604\,[616.02\,x^o\,P^{-1.974} + 17.198\,P^{-1.084}]^{0.5} \quad (8)$$

The error in G_{TH} from Equation (8) is less than 0.75% for qualities from 0.22 to 99.79% in the pressure range 28 to 100 lb./sq. in. abs. (*29*).

Cross plotting indicated that k was a function of the quantities $(1 - x^o)/x^o$ and G/G_c, both raised to approximately the same power; and the final correlating equation was

$$k = 1.465\left[\frac{1-x^o}{x^o}\cdot\frac{G}{G_c}\right]^{0.3021} \quad (9)$$

The values of the constants were determined by an iterative, nonlinear least-squares technique (*30*). The correlating curve is compared with the present and Linning's experimental data in Figure 6. All critical flow runs were excluded from the data used to develop the correlation because of the impossibility of determining the exit pressure accurately. Runs 41 and 42 also were not included on the basis of flow pattern considerations to be discussed below. Of the thirty-five data points utilized, the average deviation from the empirical curve was 7.9%, and the maximum deviation was 23%. The experimental data used to develop Equation (9) covered G/G_c ratios from 0.3 to 0.95, and the correlation should therefore be applied with caution outside this range.

It should be noted that the critical flow rates attained in this work were slightly higher than those predicted by Faletti and Moulton (*8*), again emphasizing the difficulty and importance of accurately determining the exit plane pressure. This discrepancy should not significantly affect the accuracy of the proposed correlation as long as the same method is consistently used.

Effect of Pressure

The pressure effect on the slip ratio is embodied in the correlation in the term G_c. Equation (8) shows that as pressure increases at constant quality, the critical flow rate increases, and thus by Equation (9) the slip ratio decreases. The same inverse dependency has been reported by all other investigators, and it is the expected trend if slip between the phases is promoted largely by the difference in the phase densities.

A plot of the ratio of the experimental to predicted slip ratios vs. the absolute pressure illustrated that any additional pressure effect was less than the scatter of the data.

Effect of Flow Pattern

Numerous visual studies have been made of the geometric distribution pattern of the liquid and vapor in two-phase flow, an extensive critical survey of which has been given by Vohr (*4*). Due to the subjective nature of such investigations, there is considerable variation among the various correlation techniques and results. However, the basic flow patterns are well established, and it is generally recognized that the controlling flow mechanisms vary with the flow regimes, indicating that probably no single-flow model or correlation can successfully describe the entire range of flow conditions.

Of particular significance in the present analysis is the expectation that under medium to high velocity conditions the annular flow regime should exhibit the largest slip ratios. This is due to the concentration of the liquid phase in the relatively low velocity region near the conduit wall with the vapor phase predominating in the core.

Under conditions well into the dispersed or fog flow regime, on the other hand, density stratification should play a lesser role, and local slip between entrained droplets and vapor would be expected to be the controlling factor, resulting, in general, in a lower overall average slip ratio.

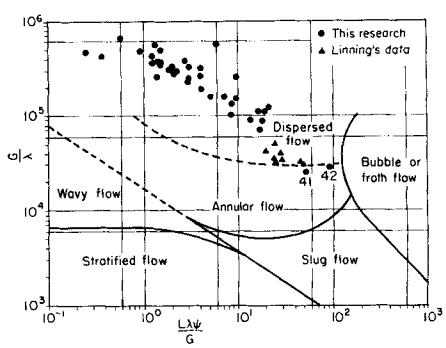

Fig. 7. Baker's flow pattern chart.

Baker's flow regime correlation (*31*), shown in Figure 7, was used to analyze the flow pattern effects on the slip-ratio data. It is important to remember when using this chart that placement of the regime transition lines is very uncertain; in fact there is no sharp transition at all, but a wide band of conditions over which the change occurs. Also, the chart was developed from two-component, non-evaporating flow data, and its validity for evaporating systems is questionable.

All runs except numbers 41 and 42 are seen to fall well within the dispersed flow region. Linning's operating conditions were closer to the annular flow regime, which would account for his slip-ratio data being somewhat higher than what would be expected from an extrapolation of the present results (Figure 6).

Runs 41 and 42 apparently lie in the annular flow region, but during both experiments a rhythmic surging effect was observed in the impulse assembly and pressure gauges, leading to the conclusion that these runs were in the transition region to the froth or possibly slug flow regimes. It was for this reason that these two runs were not included in the correlation of the rest of the data. The relatively high turbulence of these transitional regions would account for the deviation of the slip ratios for runs 41 and 42 below the trend of the rest of the data.

Effect of Quality

Practically all other investigators (*15*) have observed that the slip ratio is directly proportional to the quality, whereas the opposite effect was noted in this research. The explanation of this apparent discrepancy lies in the consideration of the flow patterns. Other measurements of slip ratios have been limited almost exclusively to void fractions less than 0.7 and consequently to flow patterns other than dispersed flow—usually the bubble, froth, or slug flow regimes. As quality increases in these regimes, the conditions generally move toward the annular flow pattern where higher slip ratios are expected. The data reported here, however, are all in the dispersed flow region where a decrease in quality shifts conditions toward the annular flow regime. Thus the two seemingly opposite effects of quality in boiling water flow and in dispersed flow are not contradictory but rather serve to emphasize the point that the controlling flow mechanisms may vary with the flow pattern.

Effect of Mass Flow Rate

As in the case of the quality, the mass velocity influenced the measured slip ratios in a manner opposite to that observed by others working in the froth, bubble, and slug flow regimes; and again flow pattern considerations provide an explanation. In the bubble or froth flow regimes, the primary mechanism causing net slip between phases is probably density stratification. Bankoff (*32*), for instance, predicted void fractions and pressure drops reasonably well with a variable density model for the bubble flow regime in which the local slip was assumed to be zero. Under such conditions, a rise in mass velocity would increase turbulence and thus increase the homogeneity of the mixture, simultaneously reducing the average slip between the phases.

Once flow conditions are completely in the dispersed region, the pressure gradient becomes the dominant mechanism affecting slip. Due to the greater density of the liquid, the static pressure gradient accelerates the vapor phase to a greater extent than the entrained droplets, causing local slip between the two phases. Under such circumstances increasing mass velocities lead to higher pressure gradients which result in larger slip ratios, as observed in this research.

Thus in a two-phase flow system the flow pattern and the mass velocity in combination are expected to determine the relative extent to which the two mechanisms, density stratification and pressure gradient (local slip), control the average slip ratio attained. The success of the ratio G/G_c in describing the present results indicates that this parameter may be a useful measure of the relative influence of these two mechanisms.

Critical Flow

There has been much conjecture recently about the value of the slip ratio at critical flow (*9, 44* to *47*). It has been suggested that the critical flow conditions could be specified mathematically by maximizing with respect to the slip ratio some gross feature of the total stream such as the momentum, kinetic energy, or entropy. Such an approach leans heavily on the assumptions of the separated flow model. Nevertheless, the resulting correlations have all been quite successful in predicting observed critical flow rates despite significant differences in the predicted slip ratios, illustrating the fact that the correlations are not very sensitive to this parameter. Pressure drop calculations, however, are quite sensitive to the value of the slip ratio at high flow rates.

The only way to resolve this argument would be to determine experimentally the momentum or kinetic energy of the stream precisely at the plane where the critical flow condition exists. The impulse plate technique is not well suited for detecting a limiting value, because reduction of the back pressure past the critical value (if it exists) would result in a continued change in the force measured at the impulse plate according to Equation (2). Thus, referring to Figure 1, P_2 would have to be measured very accurately in order to even determine if a maximum slip ratio exists. Then, to obtain its actual value, a more accurate measurement of P_1 than was possible in this research would be necessary.

Part of this problem could be circumvented, however, if a reaction balance such as that described by Stodola (*33*) were used. The reaction balance technique, although certainly more difficult experimentally, would eliminate the effect of pressure drop in the free two-phase jet beyond the exit plane and permit a confirmation of the existence or nonexistence of true critical flow conditions in the classical sense for vapor-liquid mixtures.

Effect of Metastability

The slip ratios reported here were calculated from the experimental data by assuming thermodynamic equilibrium, and they therefore reflect the effects of any metastability that may have been present.

At steam qualities greater than 0.5, Silver and Mitchell (*34*) showed that adiabatic expansion results in net condensation of vapor. High velocity flow under such conditions could lead to departures from thermodynamic equilibrium due to droplet-to-vapor heat transfer effects and to the surface tension forces associated with small, newly formed droplets (not a true metastability). If such metastable conditions arise, more of the fluid is present in the form of vapor than is expected from equilibrium theory. This results in a higher total kinetic energy, since the less dense vapor will have to move at a higher velocity to account for the same mass flow rate. The measured momentum force will thus be greater than normal, and the slip ratio, calculated from this force by assuming no metastability, will be less than the actual one. If the actual slip is already small, metastability effects could even result in calculated slip ratios less than unity. This argument offers a possible explanation of the low slip ratios obtained for the two highest quality runs of this work.

At critical flow conditions, the rapid change of pressure could conceivably result in significant departures from thermodynamic equilibrium. In a recent study of steam-

water critical flow, Cruver (*14*) detected superheating (up to 14°F.) at low qualities and supercooling (up to 7.5°) at high qualities, by using high sensitivity thermistors and a strain gauge pressure transducer to obtain simultaneous temperature and pressure measurements. In an analytical treatment of critical flow, Cruver clearly showed that metastability would significantly affect his predicted flow rates, particularly at low qualities.

It is evident therefore that metastability may be an important factor in two-phase, one-component flow systems, and further research is needed in this area.

Analysis of Pressure Drop Results

The total pressure drop over a short length of the test section extending upstream from the exit plane was obtained graphically from the pressure profile data for each two-phase run. The lengths considered were for total pressure drops of 2 lb./sq. in. or less, so that the gradients could be considered constant for calculation purposes.

The acceleration pressure drops were computed from Equation (7), by using the empirical slip-ratio correlation, Equation (9), in conjunction with Equation (A-12). Equation (6) then yielded the frictional pressure gradients, which are compared with the Martinelli-Nelson correlation (*26*) in Figure 8. The average absolute deviation from the Martinelli-Nelson curve was 36%, which is quite good when it is realized that the frictional components were obtained by difference and that the acceleration components ranged from 21 to 99% (average 70%) of the predicted total pressure gradients.

The total pressure drop is, of course, the quantity required for design purposes. The predicted total gradients, computed by adding the calculated acceleration pressure gradient to the Martinelli-Nelson frictional loss prediction (*26*), are compared with the experimental values in Figure 9. The gradients, ranging from 0.15 to 111 lb./(sq. in.)(in.), were predicted with an average absolute error of 14%; the maximum deviation was 34%.

Whereas most previous investigators have concluded that the Martinelli method is not suitable for calculating pressure drops for evaporating flows, good agreement was obtained in the present study. However almost all these workers also used Martinelli's void fraction correlation or one giving similar results to determine the acceleration pressure drop. The use of this void fraction correlation with the present data yielded calculated acceleration pressure gradients several times larger than the observed total gradients for many of the runs.

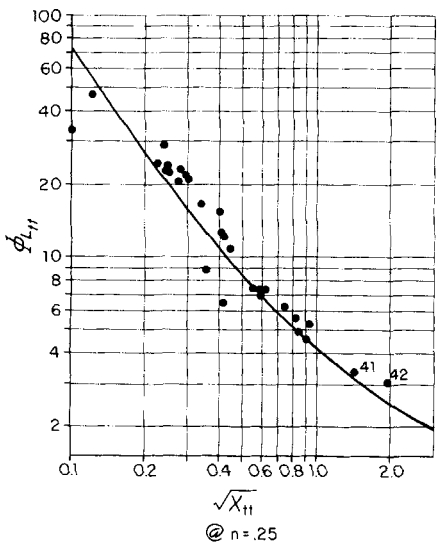

Fig. 8. Comparison of two-phase pressure drops with Martinelli-Nelson correlation.

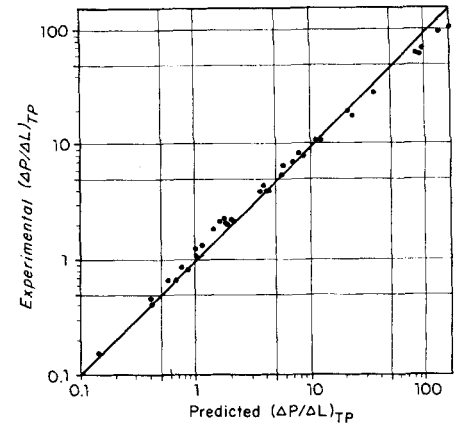

Fig. 9. Error plot of total pressure drop results.

Therefore the possibility should not be overlooked that many of the previously reported failures of the Martinelli-Nelson method to predict total pressure drops for high velocity evaporative systems may have been due at least in part to incorrect computation of the acceleration contribution to the overall pressure difference.

ANALYSIS OF LOCAL SLIP

One of the most important questions to be answered concerning two-phase flow is: How much of the average slip ratio is due to local slip between the liquid droplets and the vapor, and how much is a result of high liquid concentration along the conduit wall? Pressure gradients of over 100 lb./(sq. in.)(in.) were encountered in this investigation, and one might logically expect that considerable local slip would develop in the bulk flow. Since the runs were all in the dispersed flow regime according to Baker (Figure 7), a dispersed flow model was set up to investigate to what extent the experimental slip ratios could be accounted for by local slip alone. The following assumptions were made in the development of the model:

1. A mixture of steam and water in thermodynamic equilibrium is flowing turbulently and adiabatically in a horizontal tube.
2. The liquid is in the form of uniform sized droplets dispersed homogeneously over the tube cross section.
3. The number of droplets per unit mass of the total mixture remains constant over the test section length.
4. The droplets do not interact with each other or with the wall but only with the vapor.
5. The droplets may be treated as rigid spheres for the purpose of calculating drag. Mass transfer between the droplets and the vapor does not affect the drag.
6. The wall friction is the same as if the vapor alone were flowing in the conduit and is given by the smooth tube equation of Drew (*35*).
7. The equations of motion for each phase can be written in the one-dimensional form by using the average velocities and by neglecting interphase mass transfer. In order to simulate actual flow conditions, evaporation or condensation can be taken into account by calculating a new quality (equivalent to a new droplet diameter) after each increment of the solution (numerical integration). This greatly simplifies the resulting equations, and it is believed that little error is introduced in adiabatic systems.

These assumptions involve many gross simplifications of actual flow conditions, however the model is not intended to provide a new correlation but merely an order of magnitude study of the mechanism of local slip.

Application of the principles of the conservation of momentum and mass to each phase led to the following

equations for the variation of the average vapor and liquid velocities with position along the test section:

$$\frac{du_g}{dz} = -\frac{g_c v_g}{u_g}\cdot\frac{dp}{dz} - \frac{g_c n_d v_g F_d}{R_g \bar{v} u_g} - \frac{f u_g}{2R_g D} \qquad (10)$$

(Part 1) (Part 2) (Part 3)

$$\frac{du_l}{dz} = -\frac{g_c v_l}{u_l}\cdot\frac{dP}{dz} + \frac{6 g_c v_l F_d}{\pi \delta^3 u_l} \qquad (11)$$

(Part 4) (Part 5)

In these equations the manner in which the static pressure gradient accelerates the vapor phase more than the liquid can be seen in parts 1 and 4, since $v_g > v_l$. The drag between the droplets and the vapor is represented in parts 2 and 5, and the effect of wall friction on the vapor is reflected in part 3.

The drag force between a droplet and the vapor is given by (34)

$$F_d = \frac{\pi \delta^2 (u_g - u_l)^2 C_d}{8 g_c v_g} \qquad (12)$$

and the coefficient of drag is computed as follows:

for $(N_{Re})_d < 1.917$, $C_d = 24/(N_{Re})_d$ (Stokes law) (13)

for $1.917 \leq (N_{Re})_d < 508.4$, $C_d = 18.5/(N_{Re})_d^{0.6}$ (14)

for $508.4 \leq (N_{Re})_d$, $C_d = 0.44$ (15)

Equations (13), (14), and (15) approximate the experimentally observed relationship of drag coefficient to Reynolds number for spherical particles (36).

Equations (10) and (11) were solved numerically in the form of an initial value problem on the IBM-709 digital computer, utilizing a standard FORTRAN subprogram which employed the Runge-Kutta-Blum and Adams-Moulton forward integration techniques (37). The details of the numerical integration procedure as well as the derivations of Equations (10) and (11) are given in the original work (25).

Five experimental runs were selected for analysis. The integration for each run was started at a point 16 in. from the test section exit, using the experimental values of mass flow rate and stagnation enthalpy. The pressure profiles over the 16 in. were represented by third degree polynomials which were force fitted in sections to the experimental pressure vs. length data. Empirical equations giving the required thermodynamic properties of the vapor and liquid phases at saturation (v_g, v_l, h_l, h_{lg}, and μ_g) as a function of pressure were developed for the machine integration (25).

For each run several separate integrations were performed in which the initial droplet diameter was varied. The maximum error in either phase velocity at each iteration of the integration was maintained at less than 0.014% by automatically reducing the increment size when an estimated error of this magnitude was attained.

Results of Numerical Integration

The end results of the numerical integrations are presented in Table 1, and the entire integration for run 25 is plotted in Figure 10 along with the pressure profile used and the original pressure data. The exit plane of the test section is at $z = 16$.

For run 25 the assumed initial values of k were estimated fairly closely from preliminary integrations. It was found however that wide variations in the initial values were quickly damped out by the resulting disequilibrium in the drag and pressure gradient forces, so that the exit slip ratio obtained was barely affected. Consequently, the initial slip ratios were taken as unity for the rest of the integrations.

The most striking feature of Figure 10 is the rapid rise in slip ratio near the tube exit. The same phenomenon was observed in the integrations of runs 6 and 17. These three runs all exhibited a high, rapidly increasing pressure gradient near the tube exit. Runs 36 and 40 had low pressure gradients, and the k vs. z curves leveled off as the exit was approached.

Effect of Droplet Diameter

Since no reliable method was available for predicting the average droplet sizes, the calculations were performed for droplet diameters ranging from 10 to 200 μ. As would be expected from inertia considerations, the slip was higher for the larger droplet diameters. In no case did the droplet diameter change due to evaporation by more than 3% over the entire 16 in., and the diameter could be considered essentially constant for analysis purposes.

The droplet Reynolds and Weber numbers at the tube exit are included in Table 1. The Weber number is the ratio of the inertia forces to the surface tension forces and is usually used as a measure of the maximum drop size that can exist without breaking up into smaller droplets.

Unfortunately, there is considerable disagreement in the literature on the critical Weber number corresponding to maximum droplet size. Critical Weber numbers of 12 (38), 22 (39), and 40 to 64 (40) have been reported. Hinze (41) also pointed out that liquid droplets probably become deformed at Reynolds numbers of about 2,000, but breakup probably does not occur until Reynolds numbers of 3,000 or greater are attained.

This casts doubt on the validity of the rigid sphere assumption used in the dispersed flow model, but the slip ratios should still be of the right order of magnitude. This is borne out by the fact that the predicted exit slip ratios vary little as the droplet Weber and Reynolds numbers change over a considerable range (Table 1), again emphasizing the point that it is the pressure gradient which primarily determines the magnitude of the local slip. Based on the calculated Weber and Reynolds numbers, it was concluded that the maximum droplet sizes were probably in the range of 20 to 200 μ, depending on the pressure gradient.

Comparison with Experiment

The extent to which the local slip model corresponds to reality can be estimated by comparison with the experi-

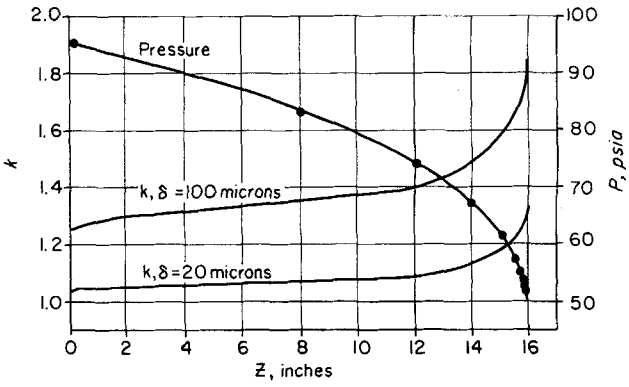

Fig. 10. Results of numerical integration of local slip differential equations, run 25.

TABLE 1. RESULTS OF NUMERICAL INTEGRATION OF DISPERSED FLOW DIFFERENTIAL EQUATIONS

Run No.	6	17	25	36	40
		Exptl. exit conditions			
x°	0.528	0.212	0.204	0.115	0.220
dP/dz, lb.$_f$/cu. in.	−32.2	−249	−21	−0.395	−0.725
G/G_c	0.85	1.2	0.73	0.31	0.29
k	1.35	3.3	2.2	2.08	1.41
		Integration results			
@$\delta = 10\mu$					
k	1.2	1.7	—	—	—
$(N_{Re})_d$	97	98	—	—	—
$(N_{We})_d$	1.9	4	—	—	—
@$\delta = 20\mu$					
k	1.38	2.04	1.32	1.04	1.05
$(N_{Re})_d$	340	272	200	11	25
$(N_{We})_d$	13	19	4.1	0.01	0.05
@$\delta = 100\mu$					
k	1.66	2.39	1.83	1.25	1.26
$(N_{Re})_d$	2600	1530	2100	340	650
$(N_{We})_d$	140	96	96	2.3	6.4
@$\delta = 200\mu$					
k	—	—	—	1.40	1.37
$(N_{Re})_d$	—	—	—	1050	1760
$(N_{We})_d$	—	—	—	11	23

mental slip ratios. The expected increased predominance of the local slip mechanism as the quality increases (corresponding to a more dispersed flow) is supported by the integration results. Run 6 was at the highest quality and was situated farthest of the five runs integrated into the dispersed flow region of Baker's chart (Figure 7). The experimental slip ratio is closely approximated by the local slip model prediction at a droplet diameter of 20 μ and with reasonable Weber and Reynolds numbers.

Run 36, on the other hand, was closest of the five to the annular flow regime, and the observed slip ratio showed the greatest deviation from that obtained with the local slip model at reasonable droplet diameters.

The highest slip ratios predicted by the model were for run 17, which was a critical run and had the largest pressure gradient. Runs 36 and 40, with the smallest pressure gradients, had the lowest calculated local slip ratios. In all but run 6, local slip could account for only a portion of the observed average slip, and it can be assumed that the remainder was due to the concentration of some of the liquid near the conduit wall (spray annular flow).

CONCLUSIONS

1. The impulse plate principle can be used to measure accurately the average slip ratios of flowing steam-water mixtures at high void fractions ($R_g > 0.7$).

2. At the high speed, dispersed flow conditions of this research, the average slip ratio decreases with increasing quality and pressure and increases with increasing mass velocity. These trends can be explained on the basis of the predominating dispersed flow pattern and high pressure gradients.

3. A simple empirical correlation of the experimental slip ratios was developed (Figure 6). It is probable, however, that a more complicated curve applies to extended ranges of the variables, and no extensive extrapolation should be made without experimental verification.

4. The experimental pressure gradients were successfully predicted by adding the acceleration component, computed with the empirical slip ratio correlation, to the frictional pressure gradient, predicted by the Martinelli-Nelson correlation.

5. An idealized dispersed droplet flow model confirmed that pressure gradient is the most important factor causing local slip between droplets and vapor. Under completely dispersed flow conditions experimental slip ratios can be almost entirely accounted for by this mechanism.

6. Near critical flow conditions, very high slip ratios may be attained in the last few millimeters of the conduit.

ACKNOWLEDGMENT

The authors wish to thank the U. S. Atomic Energy Commission for its extensive contributions to the progress of this research. The aid of the Stauffer Chemical Company and the Dow Chemical Company which provided excellent fellowships supporting this work is gratefully acknowledged.

NOTATION

A = conduit cross-sectional area, sq. ft.
B = parameter defined by Equation (4)
C_d = drag coefficient of droplets
D = diameter of conduit, ft.
f = Blasius friction factor
F = momentum force of flowing fluid, lb.$_f$
F_d = drag force between droplets and vapor, lb.$_f$
g_c = conversion factor, 32.174 lb.$_m$ ft./(lb.$_f$) (sec.^{2})
G = mass velocity, lb.$_m$/(sec.) (sq. ft.)
G_c = critical (maximum) mass velocity, lb.$_m$/(sec.) (sq. ft.)
G_{TH} = critical mass velocity predicted by homogeneous model theory, lb.$_m$/(sec.) (sq. ft.)
h,H = enthalpy, B.t.u./lb.$_m$
H° = stagnation enthalpy of flowing fluid, B.t.u./lb.$_m$
J = conversion factor, (778.16 ft.) (lb.$_f$)/B.t.u.
k = slip ratio $= u_g/u_l$
L = length in flow direction, ft.
n = constant in definition of χ_{tt}, = 0.25
n_d = number of droplets per unit mass of two-phase mixture, lb.$_m^{-1}$
$(N_{Re})_d$ = droplet Reynolds number, $= \delta(u_g - u_l)/(v_g\mu_g)$
$(N_{We})_d$ = droplet Weber number, $= \delta(u_g - u_l)^2/(g_c v_g \sigma_l)$
P = pressure, lb.$_f$/sq. ft. abs.
R = fraction of conduit cross section occupied by a fluid phase
u = average velocity, ft./sec.
v = specific volume, cu. ft./lb.$_m$
$\bar{v}$ = average specific volume, $= xv_g + (1-x)v_l$, cu. ft./lb.$_m$
w,W = mass flow rate, lb.$_m$/sec.
x = quality of two-phase mixture, $= w_g/(w_g + w_l)$
x° = homogeneous quality (assuming $k = 1$)
z = distance along test section measured from point 16 in. above exit plane, ft. or in.

Greek Letters

δ = droplet diameter, ft. or μ
Δ = finite change
μ = fluid viscosity, lb.$_m$/(ft.) (sec.)
σ = surface tension, lb.$_f$/ft.
$\Phi_{l_{tt}}$ = Martinelli parameter, ratio of actual two-phase pressure gradient to pressure gradient for liquid phase flowing alone in the test section
χ_{tt} = Martinelli parameter, $= (v_l/v_g)^{1/(2-n)} (\mu_l/\mu_g)^{n/(2-n)} (1-x)/x$

Subscripts

a = acceleration
g = vapor phase
l = liquid phase
lg = phase change

TP = total two-phase mixture
TPF = two-phase friction

Special Notation for Figure 7

G,L = mass velocities of vapor and liquid phases, respectively, lb.$_m$/(hr.)(sq. ft.)
λ = $[(\rho_g/0.075)\ (\rho_l/62.3)]^{1/2}$
μ = liquid viscosity, centipoises
ν = liquid surface tension, dynes/cm.
ρ_g,ρ_l = density of vapor and liquid phases, respectively, lb.$_m$/cu. ft.
ψ = $(73/\nu)\ [\mu(62.3/\rho_l)^2]^{1/3}$

LITERATURE CITED

1. Dougherty, D. E., *U. S. Atomic Energy Comm. Rept. TID-16750* (1960).
2. Dergarabedian, P., *J. Fluid Mech.*, **9**, 39 (1960).
3. Ambrose, T. W., *U. S. Atomic Energy Comm. Rept. HW-52927* (1957).
4. Vohr, J. H. *U. S. Atomic Energy Comm. Rept. TID-11514* (1960).
5. Cooper, M. H., *U. S. Atomic Energy Comm. Repts. UNC-5001, 5009, 5025, 5042* (1962).
6. Isbin, H. S., et al., *A.I.Ch.E. J.*, **5**, 427 (1959).
7. Gouse, S. W., *U. S. Atomic Energy Comm. Rept. NAA-SR-Memo-5597* (1960).
8. Faletti, D. W., and R. W. Moulton, *A.I.Ch.E. J.*, **9**, 247 (1963).
9. Fauske, H. K., Sc.D. thesis, Univ. Minnesota, Minneapolis (1961).
10. Zaloudek, F. R., *U. S. Atomic Energy Comm. Rept., HW-68934 REV* (1961).
11. Novoselov, V. S., *ARS J.*, **31**, 686 (1961).
12. Sjenitzer, F., *Chem. Eng. Sci.*, **17**, 309 (1962).
13. Parker, J. D., and R. J. Grosh, *U. S. Atomic Energy Comm. Rept. ANL-6291* (1961).
14. Cruver, J. E., Ph.D. thesis, Univ. Washington, Seattle (1963).
15. Lottes, P. A., et al., *U. S. Atomic Energy Comm. Rept. ANL-6561* (1962).
16. Linning, D. L., *Proc. Inst. Mech. Engrs. (London)*, **1B**, 64 (1952).
17. Smith, G. M., and Y. L. Hoe, Dominion Lab., Dept. Sci. Ind. Res., New Zealand, C. E. 174, *Rept. DL 118/6* (1956).
18. United Nuclear Corporation, *U. S. Atomic Energy Comm. Rept. NDA-2132-6* (1961).
19. Keenan, J. H., and F. G. Keyes, "Thermodynamic Properties of Steam," Wiley, New York (1936).
20. Isbin, H. S., R. H. Moen, and D. R. Mosher, *U. S. Atomic Energy Comm. Rept. AECU-2994* (1954).
21. Mosher, D. R., M.S. thesis, Univ. Minnesota, Minneapolis (1954).
22. Rayle, R. E., *Am. Soc. Mech. Engrs. Paper 59-A-234* (1959).
23. Giffen, E., and T. F. Crang, *Proc. Inst. Mech. Engrs. (London)*, **155**, 83 (1946).
24. Linning, D. L., Ph.D. thesis, Glasgow, Scotland (1950).
25. Vance, W. H., Ph.D. thesis, Univ. Washington, Seattle (1962).
26. Martinelli, R. C., and D. B. Nelson, *Trans. Am. Soc. Mech. Engrs.*, **70**, 695 (1958).
27. Levy, S., *J. Heat Transfer*, **82C**, 113 (1960).
28. von Glahn, U. H., *Natl. Aeronaut. Space Admin. TN D-1189* (1962).
29. Faletti, D. W., Ph.D. thesis, Univ. Washington, Seattle (1959).
30. Crosbie, E. A., and J. E. Monahan, *SHARE No. AN E208*, Argonne Natl. Lab., Ill. (1961).
31. Baker, O., *Oil Gas J.*, **53**, 185 (1954).
32. Bankoff, S. G., *J. Heat Transfer*, **82C**, 265 (1960).
33. Stodola, A., "Steam and Gas Turbines," trans. from 6th German ed., L. C. Loewenstein, p. 70, McGraw-Hill, New York (1927).
34. Silver, R. S., and J. A. Mitchell, *Trans. North East Coast Inst. Engrs. Shipbuilders*, **62**, 51 (1945-46).
35. Knudsen, J. G., and D. L. Katz, "Fluid Dynamics and Heat Transfer," p. 173, McGraw-Hill, New York (1958).
36. Lapple, C. E., "Fluid and Particle Mechanics," p. 282, Univ. Delaware, Newark (1951).
37. Causey, R., and W. L. Frank, "RW-INT, Adams-Moulton, Runge-Kutta Integration, 709—FORTRAN FAP Language Subroutine," Space Technol. Labs. (1958); revised at Univ. Washington Computer Lab. (1961).
38. Sofer, G., H. Firstenberg, and S. Hurwitz, *U. S. Atomic Energy Comm. Rept. NDA-2132-4* (1961).
39. Hinze, J. O., *A.I.Ch.E. J.*, **1**, 289 (1955).
40. Miesse, C. C., *Appl. Mech. Rev.*, **9**, 321 (1956).
41. Hinze, J. O., *Appl. Sci. Res. (Netherlands)*, **A1**, 273 (1949).
42. Hughmark, G. A., *Chem. Eng. Progr.*, **58**, No. 4, 62 (1962).
43. Marchaterre, J. F., and B. M. Hoglund, *Nucleonics*, **20**, No. 8, 142 (1962).
44. Moody, F. J., *J. Heat Transfer*, **87C**, 134 (1965).
45. Levy, S., *J. Heat Transfer*, **87C**, 53 (1965).
46. Cruver, J. E., and R. W. Moulton, paper presented at A.I.Ch.E. Houston meeting (February, 1965).
47. Zivi, S. M., *J. Heat Transfer*, **86C**, 247 (1964).
48. Shapiro, A. H., "Compressible Fluid Flow," pp. 73-111, Ronald Press, New York (1953).

APPENDIX

By using the one-dimensional form of the flow equations at a particular flow cross section, apply the conservation of mass principle to each phase of an equilibrium steam-water mixture flowing at steady state. For the vapor phase

$$u_g = \frac{w_g v_g}{A_g} \tag{A-1}$$

From the definitions of quality and void fraction

$$w_g = xW = xGA \tag{A-2}$$

$$A_g = R_g A \tag{A-3}$$

Substituting in Equation (A-1) yields

$$u_g = \frac{Gxv_g}{R_g} \tag{A-4}$$

Similarly, for the liquid phase

$$ul = \frac{u_g}{k} = \frac{G(1-x)v_l}{1-R_g} \tag{A-5}$$

Eliminating R_g from Equations (A-4) and (A-5)

$$u_g = G[xv_g + k(1-x)v_l] \tag{A-6}$$

$$u_l = G\left[\frac{xv_g}{k} + (1-x)v_l\right] \tag{A-7}$$

Alternatively, eliminating u_g from Equations (A-4) and (A-5)

$$R_g = \frac{xv_g}{xv_g + k(1-x)v_l} \tag{A-8}$$

$$R_l = \frac{k(1-x)v_l}{xv_g + k(1-x)v_l} = 1 - R_g \tag{A-9}$$

The total energy balance for horizontal, adiabatic, no-work flow can be expressed in the form

$$\text{H} + (\text{kinetic energy}) = \text{constant} \tag{A-10}$$

For the flow of an equilibrium steam-water mixture, Equation (A-10) may be written on a 1 lb. basis as

$$H^o = xh_g + (1-x)h_l + \frac{xu_g^2}{2g_cJ} + \frac{(1-x)u_l^2}{2g_cJ} \tag{A-11}$$

Substituting for u_g and u_l from Equations (A-6) and (A-7) and rearranging

$$x = \frac{H^o - h_l}{h_{lg}} - \frac{G^2}{2g_c J h_{lg}} \left[\frac{x v_g}{k} + (1-x) v_l \right]^2 [1 + x(k^2 - 1)] \qquad \text{(A-12)}$$

This is a cubic equation in x, and a close first approximation for its trial and error solution is calculated by setting $k = 1$ to obtain the homogeneous quality

$$x^o = \frac{H^o - h_l}{h_{lg}} - \frac{G^2 v_g^2 x^{o2}}{2g_c J h_{lg}} \qquad \text{(A-13)}$$

Manuscript received September 14, 1964; revision received July 10, 1965; paper accepted July 26, 1965.

Heat Transfer to Evaporating Refrigerants in Two-Phase Flow

J. GERARD LAVIN and EDWIN H. YOUNG

The University of Michigan, Ann Arbor, Michigan

Flow regimes occurring during evaporation of Freon-12 (dichlorodifluoromethane) and Freon-22 (monochlorodifluoromethane) inside five tubes were investigated. Two flow models are proposed, one each for vertical and horizontal tube orientation. The limits of each flow regime were determined and heat transfer correlations obtained. The most significant flow regimes were found to be nucleate boiling, annular flow, and mist flow. A correlation for the transition between annular flow and mist flow was obtained.

In previous investigations of heat transfer to refrigerants evaporating inside tubes, the greatest emphasis has been placed on obtaining bulk or overall coefficients for the complete evaporation process. There is a dearth of published information on "point" or local coefficients.

In recent years extensive studies have been made on two-phase flow, and the mechanisms involved have been more clearly defined and described. Several flow regimes have been identified and are thought to be of importance in the evaporation process. Virtually all the work reported in the literature has been carried out with fluids having physical characteristics very different from those of fluorinated hydrocarbon refrigerants, but some of the experimental data are relevant to the problem under consideration here.

The principal purposes of this investigation were to identify the important flow regimes occurring in plain tubes and tubes with internal turbulators, and to study the local heat transfer characteristics of these regimes. One plain tube and four internal fin tubes were used, and details of these are given in Figure 1 and Table 1. Both horizontal and vertical tube orientations were studied, and the working fluids were Freon-12 and Freon-22.

APPARATUS

Several basic design criteria were established for the design of the apparatus. The first of these was that the vapor-liquid mixture fed to the test section was obtained by generating and mixing two streams, one of slightly subcooled liquid and the other of superheated vapor, each stream being metered separately. Heat was generated within the walls of the test section by electrical (d.c.) resistance heating. The test section was sufficiently short to keep pressure, temperature, and vapor fraction essentially constant along it. Test section units were easily removable, since a number of them were used, and provision was made to rotate the test section from the horizontal to the vertical position.

A diagram of the apparatus is shown in Figure 2. Starting from the receiver, liquid was fed to the pump, passing through a filter-drier en route. The liquid stream leaving the pump was split into two parts, one going to the evaporator and the other to a metering section. Superheated vapor was generated in the

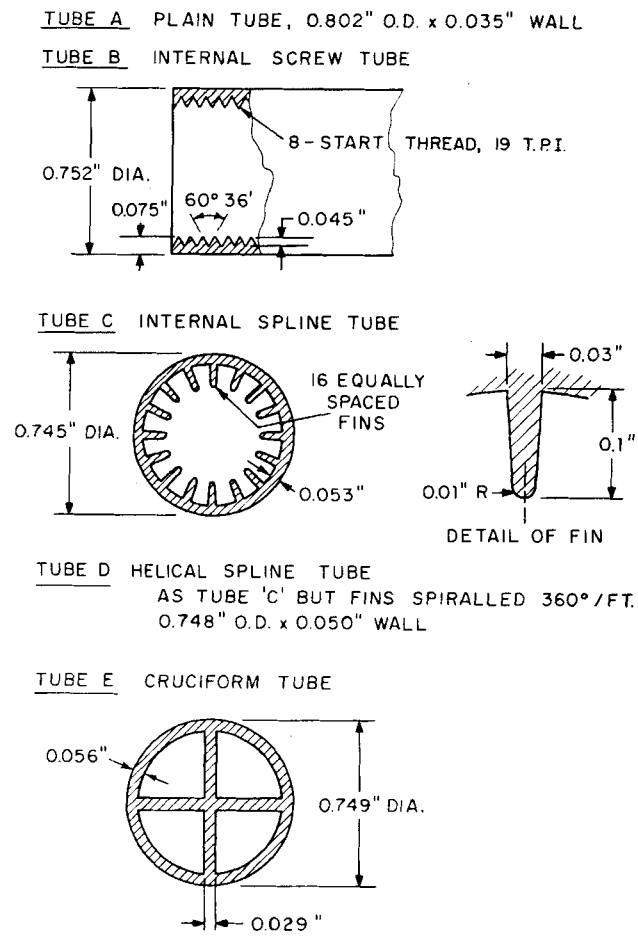

Fig. 1. Details of tubes.

J. G. Lavin is with E. I. duPont deNemours and Company, Inc., Wilmington, Delaware.